The Locating Reflectometer

P. I. SOMLO

Abstract—A microwave measuring instrument which is capable of producing a visual or graphical record of the reflection coefficient Γ along the length of a waveguide component is described. The principle of operation is the evaluation, in real time by an analog method, of the Fourier transform of Γ as a function of frequency, resulting in Γ as a function of distance.

I. Introduction

NEITHER of the two commonly used methods of time domain reflectometry is particularly suitable for measuring and determining the locations of internal reflections of commonly used waveguide components. The first of these is the conventional radar technique in which a narrow pulse is transmitted and the time lapse between the transmission of the pulse and the reception of a reflected pulse is measured. The second method consists of the transmission of a step function, and from the interference pattern of the incident and reflected waves the nature and distances of reflections may be deduced. However, this latter method runs into difficulties if waveguide modes instead of TEM modes of propagation are used. The bulk of the energy of the step function falls below the cutoff frequency of the waveguide, thus impairing the sensitivity and resolution of the method. Both of these methods require sharply rising wavefronts to provide good resolution in distance, and to measure the short time delays; when measuring nearby reflections, sophisticated detection techniques (i.e., sampling methods) must be used. The generation of these sharply rising wavefronts may be accomplished by solid-state devices, but present day technology is limited to about 50 ps in rise time, thus imposing an upper frequency limit of about 20 GHz for these pulsed methods.

Working instruments using the radar technique have been reported [8], [9] using pulsewidths of the order of 1 ns, thus limiting the resolution in distance to about 30 cm. These instruments are useful in locating reflections in long waveguide runs but cannot be used to examine internal details of reflections in a waveguide component having a total length of about 30 cm or less.

The locating reflectometer, described below, is capable of differentiating between reflections separated by approximately λ_g and does not require sharply rising wavefronts for its operation but rather a swept frequency source. In addition, it may be built to suit any waveguide system. The upper frequency limit is set only by the availability of sources and suitable crystal detectors. The electronic circuitry associated with the instrument is simple, since the bulk of the signal processing is done by the waveguide circuitry, thereby offering high stability and reliability. As a by-product, an instantaneous Smith chart presentation of the reflections is obtained, with the reference plane freely chosen.

II. Historical Background

To reduce the lower limit of the magnitude of the reflections to be measured by swept techniques, set by the finite directivity of the directional coupler used, the high-resolution swept-frequency reflectometer was designed [1]. The key to the success of this instrument lies in the physical separation of the wanted and unwanted reflections by a "long" length of waveguide. Hollway realized that the interference pattern detected by this instrument (resulting from the beating of the reflected waves from the reference reflection and from the component under test as the frequency is swept) contained all the information needed for the location of the wanted reflections. In his comparison reflectometer [2] the interference pattern is sampled at regular intervals of frequency and the Fourier transform is calculated using a digital computer. The plot of the Fourier transform is, in fact, the plot of Γ versus time, i.e., distance along a transmission line. This may be seen simply in a qualitative way since the rate of change of the interference pattern between two reflections as the frequency is swept is proportional to their separation. It was realized that an analog rather than a digital evaluation of the Fourier transform in real time would have practical advantages, and such an evaluation has been achieved by quite simple means. Two early versions of the locating reflectometer have been briefly described [3].[1]

The instrument to be described carries out the Fourier transformation at a relatively high speed and thus provides an oscilloscope display of the locations of individual reflections along the waveguide component tested.

III. Theory of Operation

A. Fourier Transform by Analog Means

It has been shown by Detlefsen [4] that the Fourier transform of the reflection coefficient as a function of frequency is the reflection coefficient as a function of time (i.e., distance along a transmission line), and proof of this will not be repeated here. Using the terminology

Manuscript received December 10, 1970; revised May 4, 1971.
The author is with the CSIRO Division of Applied Physics, National Standards Laboratory, Sydney, Australia.

[1] A short account of the experimental version of the locating reflectometer was given at a meeting of Commission I of URSI in 1969.

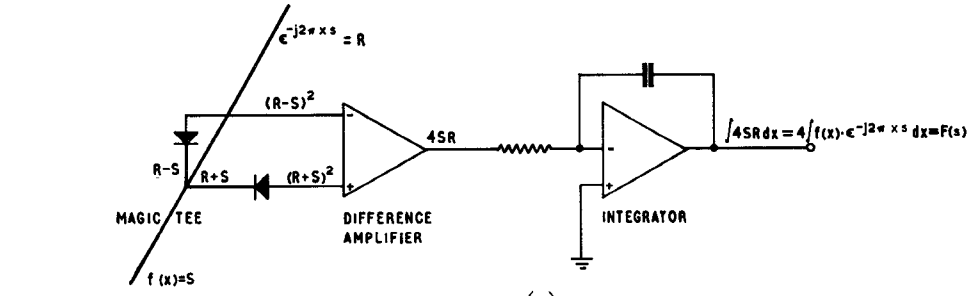

(a)

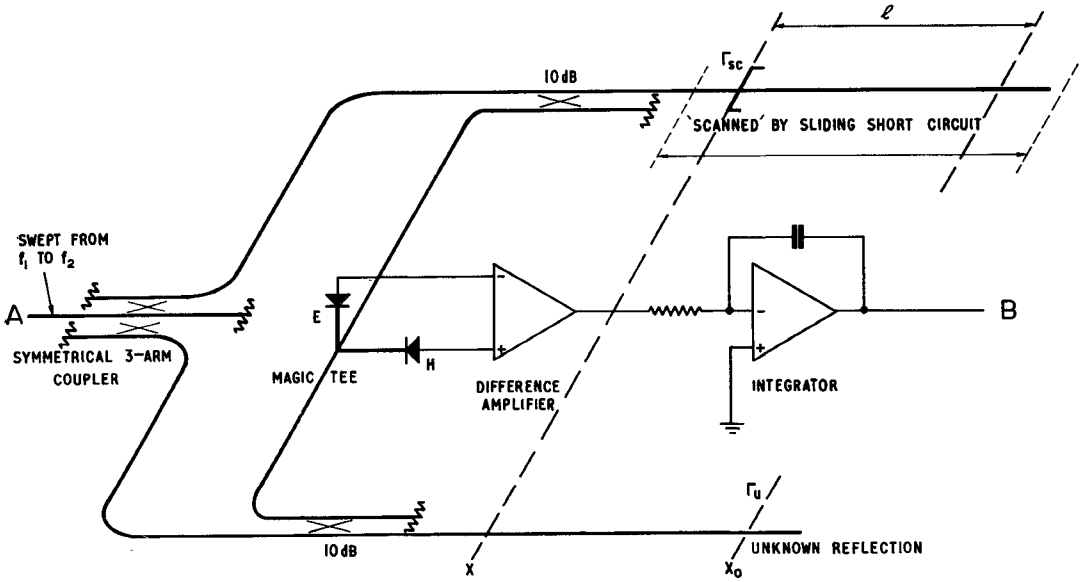

(b)

Fig. 1. (a) Basic circuit for obtaining Fourier transform by analog means. (b) Simplified schematic of locating reflectometer. Only the circuit producing Re Γ_u is shown.

of Detlefsen [4],

$$\begin{aligned}\Gamma(t') &= \int_{f=-\infty}^{f=+\infty} \Gamma(f)\cdot\exp(j2\pi ft')\,df \\ &= \int_{-\infty}^{+\infty} [\mathrm{Re}\,\Gamma(f)\cdot\cos(2\pi ft') \\ &\quad - \mathrm{Im}\,\Gamma(f)\cdot\sin(2\pi ft')]\,df \\ &\quad + j\int_{-\infty}^{+\infty} [\mathrm{Re}\,\Gamma(f)\cdot\sin(2\pi ft') \\ &\quad + \mathrm{Im}\,\Gamma(f)\cdot\cos(2\pi ft')]\,df \qquad (1)\end{aligned}$$

where $t' = 2(x_0 - x)/v_p$ is the time taken for a given phase of the signal to "travel" with the phase velocity v_p from a freely chosen reference plane x_0 to the location of a lumped reflection at x and back again to x_0. We will show, first in a simplified way and then in detail, that the circuits given in Fig. 1 do perform this Fourier transformation.

Consider the circuit in Fig. 1(a). If the two signals applied to the magic tee are of the form $\exp(-j2\pi xs)$ and $f(x)$, then, after the sum and difference of these signals are squared by the detectors and the difference of these is taken by a difference amplifier and integrated by the following stage, we obtain $4\int f(x)\exp(-j2\pi xs)\,dx$. Inspection reveals this to be the Fourier transform of $f(x)$, which is $F(s)$. This simplified approach shows the essential principle of operation of the locating reflectometer, i.e., the evaluation of the Fourier transform by analog means.

Since the signals reflected from the unknown component and the short circuit must be represented by complex quantities, a more detailed analysis is necessary. With reference to Fig. 1(b), let the signal applied to A be linearly swept from f_1 to f_2 in a repetitive fashion and be constant in amplitude. Let us assume that all microwave components are "perfect," i.e., flat in frequency response and free from internal reflections, with crystal detectors having ideal square-law characteristics. To simplify the analysis, we assume a dispersion-free transmission-line system; we shall deal with the effects of dispersion later on. In Fig. 1(b), let x_0, the freely chosen reference plane, be at the location of the unknown Γ_u in both the lower, and upper guides such that the path length from the initial split to Γ_u and back to the hybrid junction is the same as in the upper guide A to x_0 and back to the hybrid junction. The position of the sliding short circuit is at x. For the moment it is assumed that Γ_u is a single lumped reflection, independent of frequency. Then the signal reflected from the unknown Γ_u is proportional to $\Gamma_u \exp(-j\omega t)$, and the

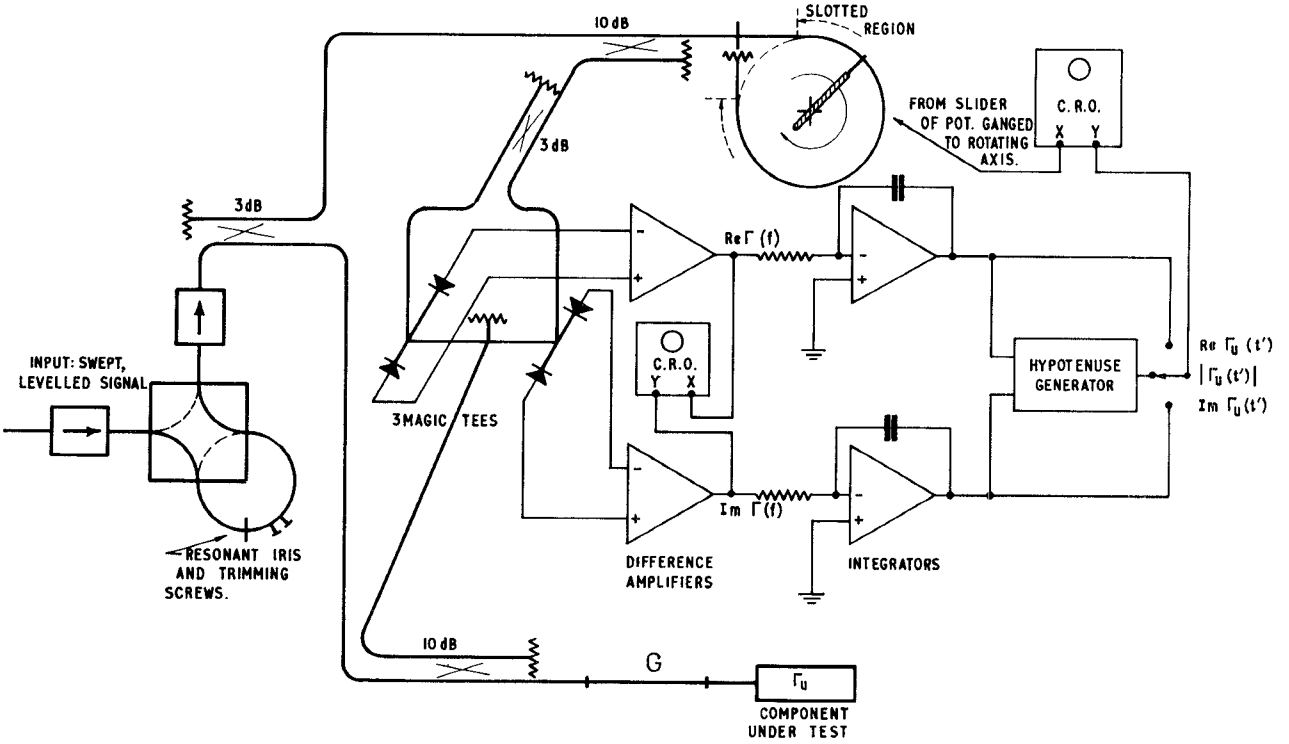

Fig. 2. Schematic of complete locating reflectometer.

signal reflected from the sliding short circuit (referred to the plane x_0) is proportional to $\Gamma_{sc} \exp(-j(\omega t + 2\omega l/v_p))$, where $l = x_0 - x$, v_p is the phase velocity, and ω is the angular frequency $2\pi f$. Because of the ability of the hybrid junction to add and subtract the entering vectors, the following signals will be present in the H and E arms:

$$V_H = \frac{1}{\sqrt{2}}\{\cos\omega t(\mathrm{Re}\,\Gamma_u - \cos a) + \sin\omega t(\mathrm{Im}\,\Gamma_u + \sin a) + j[\cos\omega t(\mathrm{Im}\,\Gamma_u + \sin a) + \sin\omega t(-\mathrm{Re}\,\Gamma_u + \cos a)]\}$$

and

$$V_E = \frac{1}{\sqrt{2}}\{\cos\omega t(\mathrm{Re}\,\Gamma_u + \cos a) + \sin\omega t(\mathrm{Im}\,\Gamma_u - \sin a) + j[\cos\omega t(\mathrm{Im}\,\Gamma_u - \sin a) + \sin\omega t(-\mathrm{Re}\,\Gamma_u - \cos a)]\} \quad (2)$$

where $a = 2\omega l/v_p$. The square-law crystal detectors on the H and E arms of the hybrid junction produce a voltage proportional to the square of the absolute value of the microwave signal reaching them. Thus we find that

$$V_H{}^{cr} = \frac{1}{\sqrt{2}}[\cos^2\omega t(\mathrm{Re}^2\,\Gamma_u + \cos^2 a - 2\,\mathrm{Re}\,\Gamma_u\cos a + \mathrm{Im}^2\,\Gamma_u + \sin^2 a + 2\,\mathrm{Im}\,\Gamma_u\sin a) + \sin^2\omega t(\mathrm{Im}^2\,\Gamma_u + \sin^2 a + 2\,\mathrm{Im}\,\Gamma_u\sin a + \mathrm{Re}^2\,\Gamma_u + \cos^2 a - 2\,\mathrm{Re}\,\Gamma_u\cos a)]$$

and

$$V_E{}^{cr} = \frac{1}{\sqrt{2}}[\cos^2\omega t(\mathrm{Re}^2\,\Gamma_u + \cos^2 a + 2\,\mathrm{Re}\,\Gamma_u\cos a + \mathrm{Im}^2\,\Gamma_u + \sin^2 a - 2\,\mathrm{Im}\,\Gamma_u\sin a) + \sin^2\omega t(\mathrm{Im}^2\,\Gamma_u + \sin^2 a - 2\,\mathrm{Im}\,\Gamma_u\sin a + \mathrm{Re}^2\,\Gamma_u + \cos^2 a + 2\,\mathrm{Re}\,\Gamma_u\cos a)]. \quad (3)$$

The two detected voltages are applied to a difference amplifier; thus the output of that stage will be $V_E{}^{cr} - V_H{}^{cr}$, which turns out to be

$$V_E{}^{cr} - V_H{}^{cr} = \frac{4}{\sqrt{2}}\left[\mathrm{Re}\,\Gamma_u\cos\frac{2\omega l}{v} - \mathrm{Im}\,\Gamma_u\sin\frac{2\omega l}{v}\right]. \quad (4)$$

Comparison of (4) and (1) reveals that $V_E{}^{cr} - V_H{}^{cr}$ is proportional to the real part of the integrand of the Fourier transform. Thus the output of the integrating stage of Fig. 1 will be $\mathrm{Re}\,\Gamma_u(t')$, the only difference being that the limits of integration are f_1 and f_2, the limits of the frequency sweep. Because $\Gamma_u(t')$ is a complex quantity, its imaginary part is also needed for its full description. It can be shown that if the "scanning function" is divided by j (90° phase shift at all frequencies), then $V_E{}^{cr} - V_H{}^{cr}$ becomes the imaginary part of the integrand of (1). For this reason both reflected signals are split equally in amplitude, as shown in Fig. 2, but the scanning function is split with a 90° phase shift by using a 3-dB coupler as the splitter, while the reflected signal from Γ_u is split symmetrically by another magic tee. The in-phase and quadrature scanning functions are used in two magic tees (with their correspond-

ing detectors and electronic stages) to produce the real and imaginary parts of the Fourier transform of $\Gamma_u(f)$, resulting in $\Gamma_u(r')$.

References [2]–[4] have given experimental and theoretical proofs that the plot of $|\Gamma_u|$ as a function of distance given by this type of instrument, will have the shape of the $|\text{sinc}|$ function, defined as $|\sin x/x|$. This result is the natural consequence of dealing with an instrument having a (stipulated) flat-frequency response and obtaining the Fourier transform of a reflection Γ_u, which is constant between the sweep limits of f_1 and f_2 and zero outside these limits. It is well known that the Fourier transform of a rectangular pulse is the sinc function (here, however, the pulse is in the frequency domain, and the Fourier transform is in the time domain).

Equation (4) reveals that $V_E^{cr} - V_H^{cr}$ is the real part of Γ_u, as would be measured at l, and we have seen that the other magic tee and associated circuitry produces the imaginary part of Γ_u at l. Therefore, if the outputs of the two difference amplifiers are connected to the X and Y plates of an oscilloscope, a swept frequency Smith chart representation of Γ_u results with the reference plane chosen by the position of the sliding short-circuit.

As a point of interest, it is worth noting that the instrument would also perform its locating function if supplied with white noise, or a closely spaced static "comb" of frequencies. In this mode of operation the locating signal would be available before the integrators, thereby simplifying the instrument. This mode of operation may be likened to a multiplying correlating receiver or to a white-light interferometer [7].

B. The Effects of Waveguide Dispersion

We have seen that the hybrid junction of Fig. 1 responds to the phases of the applied microwave signals. For this reason, for fixed positions of the sliding short circuit and of the unknown reflection, the number of zero crossings of (4) is governed by the change in the phase velocity v_p for a given change in frequency when sweeping from f_1 to f_2. Because of waveguide dispersion, the change in v_p (or in guide wavelength λ_g) is greater than the corresponding change in frequency. For example, at X band λ_g changes by a factor of nearly 2 for a frequency change of 8.2 to 12.4 GHz. Thus one of the effects of waveguide dispersion is to widen the effective swept bandwidth. Numerical evaluation by a digital computer of $|\Gamma_u(t')|$, taking dispersion into account, confirmed that the axial resolution of the instrument is 2.52 cm when sweeping from 8.2 to 12.4 GHz, while such a resolution would be obtained in a TEM (dispersion-free) system with a total bandwidth of 6.6 GHz. (The definition adopted here for the axial resolution is the half-width of the main lobe of the $|\text{sinc}|$ function when locating a single lumped reflection.) The same calculation has shown that another effect of the dispersion is a slight distortion of the sidelobes of the $|\text{sinc}|$ function, which is the plot of $|\Gamma_u|$ versus distance given by the instrument, but this in no way affects the locating capability of the instrument.

C. Locating Frequency Dependent Reflections

In the above it was assumed that the reflections detected are independent of frequency. In practice this is rarely the case. However, it has been shown [4] that simple (single-reactive component) frequency-dependent reflections are located correctly. Frequency dependence manifests itself as distortion of the sidelobes of the $|\text{sinc}|$ function. As will be described later, the sidelobes are suppressed by the shaping function; thus for most practical cases the effect is not noticeable. However, one has to remember that the Fourier transformation involves the integration from f_1 to f_2; thus a weighted (due to shaping) averaging of $\Gamma(f)$ takes place. If the nature of the unknown is such that it sets up reflections only in a narrow frequency band, both the sensitivity and the axial resolution will be reduced. However, by switching to the Smith chart mode of operation, the correct magnitude of the reflection at any frequency may be obtained.

The indicated positions of reflections are referred to positions along a uniform waveguide due to the scanning in the upper guide in Fig. 2. Thus, reflections seen through a "delay line" (a low-pass filter or a flexible guide, for instance) will appear further away, corresponding to the electrical and not the physical positions of the reflections.

IV. Construction of the Instrument

The locating reflectometer was built for operation in the X band (8.2–12.4 GHz) and, with the following exceptions, commercially available components were used.

A. The Hybrid Tees

The three hybrid tees were constructed in one block, machined out of four pieces of brass. All three junctions were broad banded by placing a suitably shaped object in the junction area, resulting in $|\Gamma_{tee}| < 0.2$ for $9 \leq f \leq 12$ GHz. The role of the tees is merely that of phase detection; therefore a particularly high degree of match is not required.

B. The Mechanical Scanning of the Reference Guide

In [3] the scanning was accomplished by a noncontacting short circuit pulled by the carriage of the X–Y recorder. However, for an oscilloscope display this method is unsuitable. The present instrument uses a circularly curved slotted waveguide in which a highly reflective antenna is repetitively moved through $\frac{3}{4}$ of a turn by a small electric motor. A potentiometer ganged to the rotating antenna shaft provides the X deflection

of the oscilloscope, or chart recorder (see Fig. 2). Since the sensitivity of the instrument is proportional to the magnitude of the scanning reflection, as shown by (1), an antenna is used that causes almost full reflection. It was found that a loop of conductive wire with about $\lambda_g/8$ separation produces almost full reflection independent of frequency when fully immersed into a rectangular guide through a central broad-wall slot. The guide contains a matched load at its end to prevent reflections (resonances) in the scanning guide, and the load effectively zeros the scanning function at the end of the scan when the loop is absent from the guide. The length of the scanned waveguide is about 53 cm. The constancy of the antenna reflection with scan was proved to be better than 1 percent.

There is no lower limit to the scanning speed. In fact, the antenna may be stopped at any point, and either the reflection at the corresponding distance in the measuring guide or the Smith chart referred to that plane may be examined in detail. However, the upper limit of the scanning rate is determined by the sweep repetition rate of the signal generator used. The Fourier transform of (1) requires an integral to be evaluated over the full frequency range for any value of $\Gamma(t')$. If the scanning is done too rapidly, there is an appreciable change in $\Gamma(f)$ before the integral is evaluated, resulting in reduced sensitivity and reduced axial resolution. With a commercial X-band sweep generator having a sweep repetition rate of about 50 Hz, a 10-percent drop in indicated sensitivity occurs at a scanning rate of about 15 cm/s, i.e., when the distance covered by the mechanical scan during one sweep cycle is about 10 percent of the resolution in distance as defined above.

C. The Realization of the Shaping Function

The theoretical reasons for using a shaping function are given in [2] and are identical with those used in the design of radio-telescope antennas when sidelobe suppression is required. In [2] and [4] the shaping function is used to multiply the observed frequency response of Γ_u in the course of the digital computation in order to reduce the sidelobes of the $|\text{sinc}|$ function, which is the Fourier transform of a rectangular pulse, i.e., of a constant Γ_u from f_1 to f_2 and zero outside these limits. In the locating reflectometer the shaping function is applied to the overall frequency response of the instrument by means of a resonant iris. The iris, placed between two isolators, is tuned to the midband frequency and has an equivalent Q factor of about 5. The shaping function is trimmed by two tuning screws, located close to the resonant iris, which are adjusted while observing the display of a single reflection. In this way the overall frequency response of the system is optimized (i.e., suitably shaped) to include the effects of imperfect leveling, detector-response characteristics, etc. Once the best compromise between the narrowness of the main lobe and the amount of sidelobe suppression has been found, the screws are locked and require no further adjustment. For Smith chart displays the shaping function is switched out of the circuit (see Fig. 2).

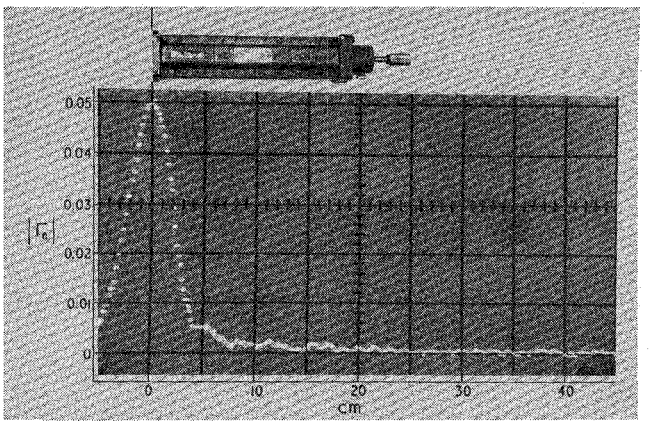

Fig. 3. Photograph of, and corresponding locating display of a calibrating reflection $|\Gamma_c| = 0.05$.

D. The Electronic Circuitry

The electronic circuits associated with the locating reflectometer are inherently simple. Four crystal detector buffer amplifiers feed two difference amplifiers, at the outputs of which the signals for Smith chart display are available. These signals are integrated during each sweep yielding Re $\Gamma_u(t')$ and Im $\Gamma_u(t')$. At the onset of the flyback of the signal generator sweep, the outputs of the integrators are sampled and held until the next flyback. During flyback the integrating capacitors are discharged to zero, ready for the next sweep. For plotting $|\Gamma_u|$ an improved version [6] of a hypotenuse generator [5] is used.

V. Results and Accuracy

The main use of the locating reflectometer is in the location of reflections in waveguide components. As we have seen, in order to identify the locations of reflections the frequency is continuously swept; therefore, on the plots given by the instrument, the vertical axis denoting $|\Gamma_u|$ is a weighted (due to shaping) average of $|\Gamma_u|$ in the frequency band. If the exact value of Γ_u at any frequency is of interest, the Smith chart mode of operation yields this, but, of course, does not provide any locating information. However, examining a particular waveguide component by both the locating and the Smith chart modes of operation of the instrument, a great deal may be learned about the reflection characteristics of the component under test.

A. Locating Reflections in Waveguide Components

The instrument is first calibrated by connecting a known reflection to the measuring port. In Fig. 3 the calibrating reflection is $|\Gamma_c| = 0.05$, and the gains of the Re Γ and Im Γ amplifiers were adjusted to produce a

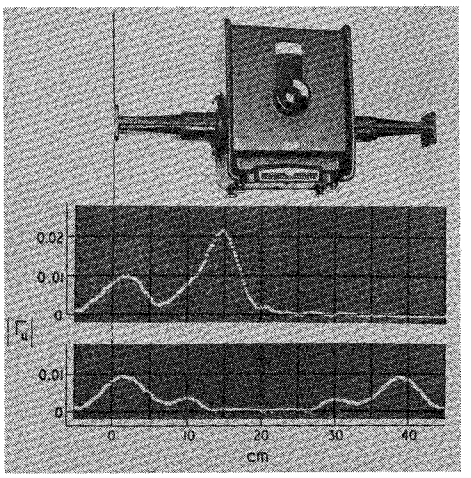

Fig. 4. Internal reflections of a rotary vane attenuator. Lower trace: attenuator set to minimum attenuation; upper trace: attenuator set to maximum attenuation.

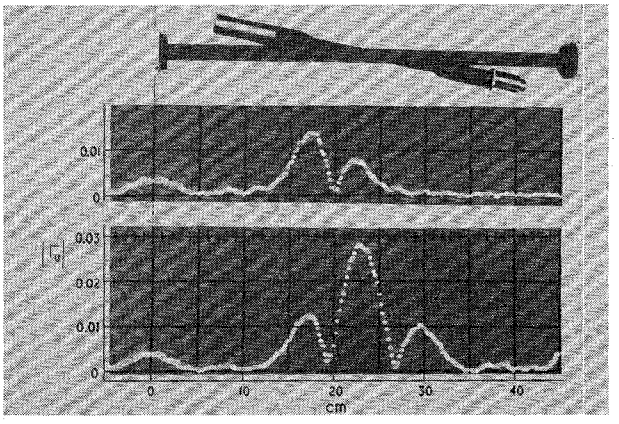

Fig. 5. Internal reflections of a gas-discharge noise source. Lower trace: unfired condition; upper trace: fired condition.

5-cm deflection at the location of Γ_c. For all the examples given, the horizontal scale was adjusted to be 5 cm in guide for 1 cm on the screen. It may be seen that the traces are made up of a series of dots, each dot corresponding to one sweep cycle of the sweep generator.

Fig. 4 shows the locations of internal reflections in a rotary-vane attenuator set to minimum and maximum attenuation. Note that when set to "max," reflections beyond the attenuating section are not registered. Fig. 5 shows a gas-discharge noise source when switched on and off. When it is switched on, reflections further away are not registered because of the attenuation through the plasma. Fig. 6 shows that in a slide-screw tuner with the probe fully withdrawn, there are two reflections of about $|\Gamma_u| = 0.006$ each, located at the two ends of the slotted section.

The ability of the locating reflectometer to measure and locate very small reflections is demonstrated by increasing the oscilloscope vertical sensitivity to $|\Gamma_u| = 0.001$/cm, as in the following examples. Fig. 7 illustrates a 20-cm guide joined by a "good" flange to another section of guide. The flange produces a reflection of $|\Gamma_u| = 0.002$. In fact, it was found that it is extremely rare to make a flange connection that is not detectable by the instrument when using commercially available components. Fig. 8 indicates the internal reflections

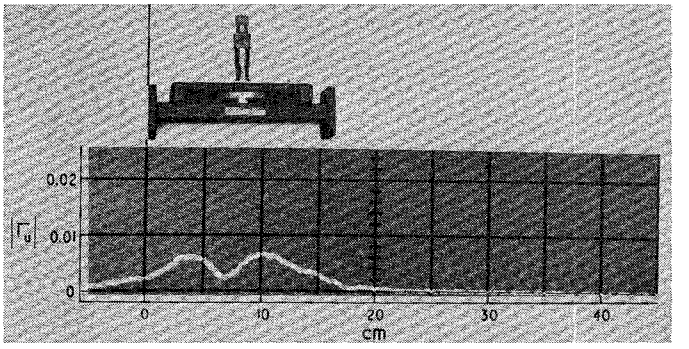

Fig. 6. Internal reflections of slide-screw tuner with probe fully withdrawn.

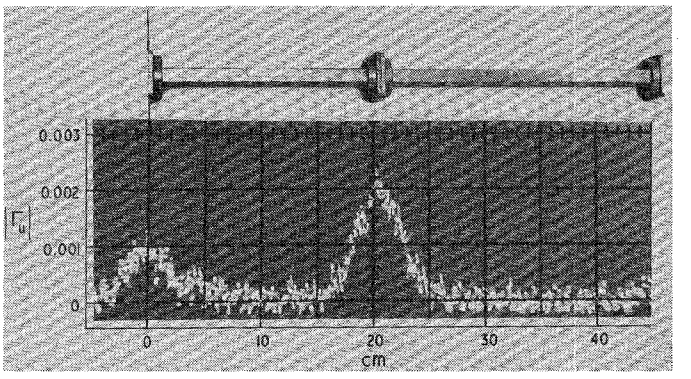

Fig. 7. Detection of "laboratory quality" flange reflection. A 20-cm guide connected by a flange to a longer section of guide.

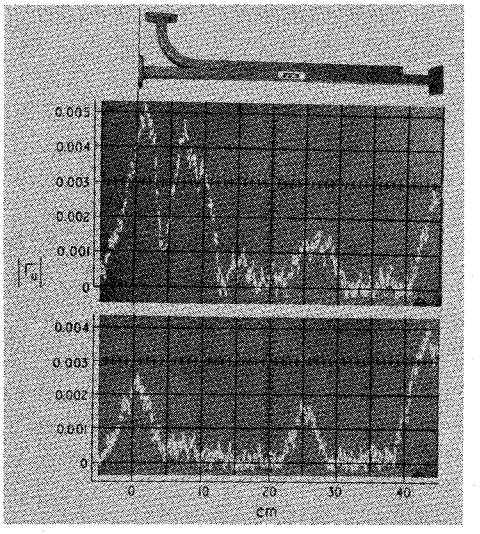

Fig. 8. Locations of reflections in 3-dB multihole coupler. Lower trace: straight arm; upper trace: curved arm connected to the measuring flange of the instrument.

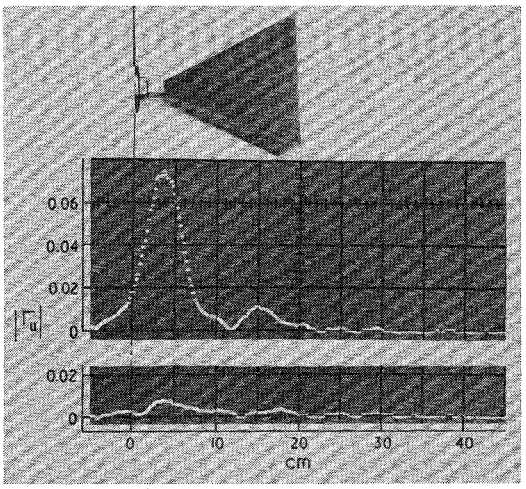

Fig. 9. Reflections inside horn antenna. Upper trace: uncompensated horn; lower trace: compensated near the planes of the individual reflections (see Section V-B).

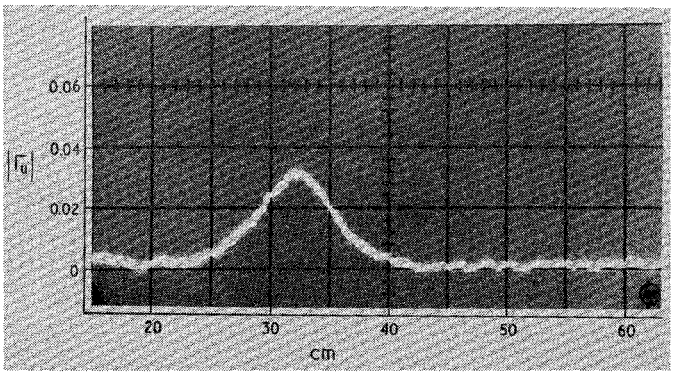

Fig. 10. Reflections located in air. A sample sheet of absorbing material was held about 32 cm in front of the horn antenna shown in Fig. 9.

along the straight and curved arms of a high-quality 3-dB directional coupler. Note the two reflections in the curved arm at the beginning and end of the curved section. Some reflections at the end of the coupling region are also present, but it is most likely that some of the reflection shown is caused by the matched termination in the curved arm. Flange reflections at both ends are clearly demonstrated. It has been found that directional couplers of identical make and model have different amounts of internal reflections.

B. Special Applications

Fig. 9 shows a waveguide horn antenna. The upper diagram shows a large reflection of about $|\Gamma_u| = 0.07$ set up by the sudden discontinuity at the start of the horn. A smaller reflection of about $|\Gamma_u| = 0.01$ is located just inside the open aperture. Using the locating capability of the instrument, it was possible to compensate these reflections individually near the planes where they occur. Small metallic objects (ball bearings moved by external magnets) were glued into the antenna after their optimum positions had been found by observing the locating display. The compensated antenna exhibits reflections of $|\Gamma_u| < 0.01$ over a wide frequency band, manifested by Fig. 9, since the locating display is a result of a wide-band analysis of the reflections.

When the horn of Fig. 9 is connected to the instrument, the space in front of the antenna may be examined for reflections. Fig. 10 is a display of reflections from an absorbing material (used to line anechoic chambers) placed about 32 cm in front of the horn. The importance of this mode of operation is that accurate comparative measurements of absorbing materials may be carried out in an ordinary laboratory with no special precautions taken to reduce reflections from the walls and from laboratory equipment in the vicinity. As Fig. 10 shows, room reflections and other reflections outside the 53 cm of scanned region are completely ignored by the instrument.

If the outputs of the integrating stages producing Re $\Gamma_u(t')$ and Im $\Gamma_u(t')$ are connected to the X and Y plates of an oscilloscope, a "Smith chart in the time domain" representation results (which is distinctly different from the conventional Smith chart display which is in the frequency domain). This mode of operation is particularly useful when we wish to investigate the phase angles of individual reflections in the presence of other reflections at least a few wavelengths away. In such a case, a conventional Smith chart is too complicated to show the nature of the reflection considered, whereas, the Smith chart in the time domain (i.e., distance domain) produces a single point on the oscilloscope for a full frequency sweep for any fixed position of the scanning reflection.

C. Accuracy

If the instrument is calibrated by a known standard reflection, then in the neighborhood of the calibrating reflection the accuracy is limited by the standard used. Commercially available standard waveguide reflections are within 5 percent of the nominal value of the reflection; thus in a located reflection of $|\Gamma_u| = 0.01$, the error due to calibration may amount to 0.0005. The scale of the reflection coefficient displayed is linear as long as the crystal detectors are operated in the square-law region. The lower limit of detectable reflections is set by the crystal detector and amplifier noise amounting to about 0.0002 in reflection coefficient as shown by the noise of Figs. 7 and 8. (Directional coupler directivity does not affect the results in the locating mode because of the physical separation of these reflections from Γ_u.)

The axial resolution (when sweeping the full X band and using a shaping function to suppress the sidelobes) is shown by Fig. 3 to be about 4 cm (about one λ_g at midband) when defined as the half width of the main-lobe. However, when using an X–Y plotter on a 1:1

distance scale, single reflections may be located to an accuracy of about 0.1 cm.

When obtaining a Smith chart display of reflections at a fixed frequency, instrument errors may be canceled by altering the differential gains of the difference amplifier to shift the point corresponding to a perfectly matched load (the center of the circle traced by a sliding load) exactly into the center of the screen.

VI. Summary

A swept-frequency instrument has been described, capable of producing either a visual or a permanent record of reflections along waveguide components or in space. Individual reflections in the range $|\Gamma| = 0.0005$ to full reflections may be indicated both in position and in magnitude and phase. There is no inherent upper frequency limitation to the technique; therefore instruments can be constructed to operate in any waveguide-size system. As a by-product, a single frequency or swept Smith chart display is available referred to a freely chosen plane.

Acknowledgment

The author wishes to thank Dr. D. L. Hollway and I. G. Morgan for their helpful discussions and P. W. Campbell, who manufactured the special waveguide components.

References

[1] D. L. Hollway and P. I. Somlo, "A high-resolution swept-frequency reflectometer," *IEEE Trans. Microwave Theory Tech.*, vol. MTT-17, Apr. 1969, pp. 185–188.
[2] D. L. Hollway, "The comparison reflectometer," *IEEE Trans. Microwave Theory Tech.*, vol. MTT-15, Apr. 1967, pp. 250–259.
[3] P. I. Somlo and D. L. Hollway, "Microwave locating reflectometer," *Electron. Lett.*, vol. 5, Oct. 1969, pp. 468–469.
[4] J. Detlefsen, "Frequency response of input impedance implies the distribution of discontinuities of a transmission-line system," *Electron. Lett.*, vol. 6, Feb. 1970, pp. 67–69.
[5] D. P. Franklin, "Hypotenuse function generator," *Electron. Eng.* (London), vol. 41, Jan. 1969, pp. 63–65.
[6] D. L. Hollway, "An improved hypotenuse function generator," to be published.
[7] H. A. Gebbie, C. F. Osborne, N. W. B. Stone, and B. K. Taylor, "The NPL teramet," *Engineer* (London), Oct. 1968.
[8] C. E. Muehe, "Band-pass time-domain reflectometry," *IEEE Int. Conv. Rec.*, 1969, pp. 416–417.
[9] Hewlett-Packard Co., "Narroband TDR locates waveguide faults," *Microwave J.*, vol. 13, Dec. 1970, p. 16.

Theory and Operation of a Reciprocal Faraday-Rotation Phase Shifter

WILLIAM E. HORD, MEMBER, IEEE, FRED J. ROSENBAUM, SENIOR MEMBER, IEEE, AND JAMES A. BENET, MEMBER, IEEE

Abstract—**The operation of a longitudinally magnetized fully filled square-waveguide reciprocal-ferrite phase shifter is described. The frequency characteristics of the phase shifter are predicted and measured. An error analysis, including rotational errors incurred in wide-band operation and manufacturing tolerances, is used to predict the loss performance of the device. The effect of the ferrite parameters and the waveguide geometry on phase-shifter performance may be calculated using this analysis. The variation of the phase shift with temperature as well as high-power effects are presented, and design considerations, including choice of ferrite saturation magnetization for wide-band performance, are discussed. Experimental results closely confirm the key aspects of this theory.**

Manuscript received December 22, 1970; revised June 6, 1971.
W. E. Hord is with the Department of Engineering, Southern Illinois University, Edwardsville, Ill. 62025, and the Emerson Electric Company, St. Louis, Mo.
F. J. Rosenbaum is with the Department of Electrical Engineering, Washington University, St. Louis, Mo., and is a Consultant to the Emerson Electric Company, St. Louis, Mo.
J. A. Benet is with Spartan Manufacturing Company, Flora, Ill.

I. Introduction

ALTHOUGH ferrite-loaded waveguiding structures have long been used as phase-shifting elements [1]–[7], design procedures for reciprocal phase shifters have remained largely empirical. The principle reason is that the ferrite–microwave field interaction in many useful phase-shifter geometries cannot be calculated exactly. An excellent example is the Reggia–Spencer device in which a longitudinally magnetized ferrite